Multiscale structural analysis of mouse lingual myoarchitecture employing diffusion spectrum magnetic resonance imaging and multiphoton microscopy

Citation: Gaige, Terry A. et al. "Multiscale structural analysis of mouse lingual myoarchitecture employing diffusion spectrum magnetic resonance imaging and multiphoton microscopy." Journal of Biomedical Optics 13.6 (2008): 064005-8. ©2008 SPIE

As Published: http://dx.doi.org/10.1117/1.3046724

Publisher: SPIE

Persistent URL: http://hdl.handle.net/1721.1/60030

Version: Final published version: final published article, as it appeared in a journal, conference proceedings, or other formally published context

Multiscale structural analysis of mouse lingual myoarchitecture employing diffusion spectrum magnetic resonance imaging and multiphoton microscopy

Terry A. Gaige
Hyuk Sang Kwon
Guangping Dai
Victor C. Cabral
Ruopeng Wang
Yoon Sung Nam
Bevin P. Engelward
Van J Wedeen
Peter T. C. So
Richard J. Gilbert
Massachusetts Institute of Technology
Department of Mechanical and Biological Engineering
Cambridge, Massachusetts 02139
and
Massachusetts General Hospital
Athinoula A. Martinos Center for Biomedical Imaging
Charlestown, Massachusetts 02129

Abstract. The tongue consists of a complex, multiscale array of myofibers that comprise the anatomical underpinning of lingual mechanical function. 3-D myoarchitecture was imaged in mouse tongues with diffusion spectrum magnetic resonance imaging (DSI) at 9.4 T (b_{max} 7000 s/mm, 150-μm isotropic voxels), a method that derives the preferential diffusion of water/voxel, and high-throughput (10 fps) two-photon microscope (TPM). Net fiber alignment was represented for each method in terms of the local maxima of an orientational distribution function (ODF) derived from the local diffusion (DSI) and 3-D structural autocorrelation (TPM), respectively. Mesoscale myofiber tracts were generated by alignment of the principal orientation vectors of the ODFs. These data revealed a consistent relationship between the properties of the respective ODFs and the virtual superimposition of the distributed mesoscale myofiber tracts. The identification of a mesoscale anatomical construct, which specifically links the microscopic and macroscopic spatial scales, provides a method for relating the orientation and distribution of cells and subcellular components with overall tissue morphology, thus contributing to the development of multiscale methods for mechanical analysis. [DOI: 10.1117/1.3046724]

Keywords: multiscale imaging; biomedical optics; multiphoton microscopy; diffusion weighted magnetic resonance imaging; second-harmonic generation; tissue morphology.

Paper 08024R received Jan. 18, 2008; revised manuscript received Aug. 9, 2008; accepted for publication Aug. 24, 2008; published online Jan. 5, 2009.

1 Introduction

Understanding biological structure-function relationships in muscular organs requires a method to image fiber organization across multiple spatial scales. This question is particularly challenging in cases where the tissue's myoarchitecture exhibits complex geometries, such as crossing, convergence, or helicity. Examples of such tissues include the tongue,[1,2] heart,[3] vasculature,[4] and gastrointestinal tract.[5] We have previously demonstrated the feasibility of imaging 3-D myoarchitecture in whole tissues through the use of diffusion spectrum magnetic resonance imaging (DSI),[6,7] a method that resolves the orientation of complex multifiber arrays by the identification of one or multiple diffusion maxima per voxel. These diffusion maxima may also be associated into mesoscale constructs (myofiber tracts) defined by the angular similarity exhibited by the principal diffusion vectors in multiple adjacent voxels.[8] On the basis of these formulations, we have postulated that tissue myoarchitecture may be depicted as an array of variably aligned myofiber tracts, which, in concert, comprise a mesoscale template for local tissue contractility.

In order to explicitly relate fiber orientation across microscopic (single cell) and mesoscopic (multicell arrays) scales, we compare herein the local orientation distribution of myofibers imaged with 9.4 T DSI and high-speed 3-D two-photon microscopy (TPM).[9] The orientational distribution of fibers obtained through DSI reflects the principal directions and permeabilities of the constituting cell membranes and fluid compartments,[10] whereas the orientational distribution obtained from TPM reflects the morphology and mean alignment of individual myocytes and contained myofilaments imaged via second harmonic generation (SHG) from the intracellular myosin array.[11] We propose that the specific orientational distribution function (ODF) for fiber alignment, derived either from DSI or TPM, constitutes a common metric by which fiber orientation can be related at the scale of the single cell, multicellular array, and the tissue. The tongue is a particularly interesting model for this form of study because we have previously determined, in both *in vitro*,[6,7,12] and *in vivo*[13] studies, that its myoarchitecture contains continuous arrays of crossing fibers, and we have inferred from its underlying structure the basis for its physiological deformations.[14–16] We have specifically shown in the case of the tongue the capacity to derive net microscopic fiber orien-

Address all correspondence to: Richard J. Gilbert, M.D., Department of Mechanical Engineering, Massachusetts Institute of Technology, 77 Massachusetts Avenue, Cambridge, MA 02139. Tel: (617) 620-2032; Fax: (781) 622-5090; Email: rgilbert@mit.edu.

1083-3668/2008/13(6)/064005/8/$25.00 © 2008 SPIE

tation employing TPM and autocorrelation analysis in the case of single fields of view.[17] Although such analyses had a predictable relationship with the associated principal eigenvectors for diffusion obtained via diffusion tensor imaging (DTI) for a given imaging field, this work did not assimilate this information into a form which could be used to assess whole tissue myoarchitecture.

Our goal in the current work was to develop a method, combining microscopic and diffusion weighted imaging tools, for explicitly determining the 3-D alignment of myofibers at the cellular scale in relationship to the orientation of cellular arrays at the scale of the whole tissue. Such multiscale structural analyses display in quantitative geometric terms the 3-D resolved geometry of complex tissues and thus provide a means by which global mechanical function may be projected from its microscopic and mesoscopic underpinnings. Furthermore, the correlation of mesoscale fibers with the underlying cellular structures may provide a molecular-level understanding of fiber function.

2 Materials and Methods

2.1 *General Methods*

Imaging experiments were performed on four whole anterior tongues, which were excised from female 357BL ($n=3$) and FYDR-Rec mice ($n=1$) adult mice employing high-field (9.4 T) DSI and a TPM system embodying high throughput (10 fps) and a computer-controlled specimen stage and microtome. Location-specific orientational distribution functions were obtained and streamline tractography performed in both instances in order to generate comparable mesoscale ODFs and myofiber tracts.

2.2 *Handling of Tissue Specimens*

The specimens for study consisted of the anterior 2/3 of the tongues excised from 357BL and FYDR-Rec mice. Imaging was performed on the same tissues, employing DSI tractography and TPM in sequence. Once excised, the tissue samples were placed within 1 h of harvest in buffered neutral 10% formalin to achieve fixation. These samples were brought in fixative to the nuclear magnetic resonance (NMR) imaging facility, where DSI experiments were carried out. Within 48 h of the DSI experiment, the tissues were embedded in paraffin using an automated tissue processor (Leica).

2.3 *High-Field Diffusion Spectrum Imaging of the Mouse Tongue*

DSI derives a complete probability density function for diffusing hydrogen atoms per voxel, thus mapping the likelihood that a model particle will diffuse a particular distance and direction within a given period of time. Directions of greatest diffusion correspond to the orientation of the long axis of fiberlike cells. The probability density function (pdf) is represented by a mathematical expression termed the average diffusion propagator ($\bar{P}s$), which is the sum of the probability density functions for each possible proton spin position and weighted by the proton density distribution. Stejskal and Tanner[18] related $\bar{P}s(R|\Delta)$ to the amount of signal attenuation for an applied diffusion weighting gradient $\mathbf{g}$ and diffusion duration Δ

$$M(\mathbf{q},\Delta) = M(\mathbf{0},\Delta)\int \bar{P}s(R|\Delta)e^{(iq\cdot R)dR} \qquad (1)$$

$$\mathbf{q} = \gamma \mathbf{g}\delta,$$

where $\mathbf{q}$ is called the q value, γ is the proton gyromagnetic ratio, M is the signal intensity, δ is the diffusion pulse duration, and R is the diffusion distance. The b value defines the maximum diffusion weighting for a set of diffusion weighted image acquisitions as follows:

$$b = \|\mathbf{q}_{\max}^2\|\Delta. \qquad (2)$$

Equation (1) demonstrates that a Fourier relationship exists between the diffusion weighted signal in q space and the 3-D probability distribution function. Diffusion weighted images are acquired for a set of q values and the pdf is reconstructed by

$$\bar{P}s(R,\Delta) = F^{-1}[M(\mathbf{q},\Delta)], \qquad (3)$$

where F^{-1} denotes the inverse Fourier transform. The spacing between $\mathbf{q}$ vectors defines the field of view and the maximum $\mathbf{q}$ vector defines the resolution of the pdf. To convert the data from a 3-D image volume to a contour surface, the pdf is integrated radially and weighted by the magnitude of R

$$\mathrm{ODF}(\mathbf{u}) = \int \bar{P}s(\rho\mathbf{u})\rho\mathbf{u}d\rho, \qquad (4)$$

where ρ and $\mathbf{u}$ are the magnitude and unit vector describing R. The result, normalized by the minimum and maximum range of diffusion values per voxel to accentuate topology, describes the underlying fiber architecture and is termed the ODF.

Magnetic resonance imaging (MRI) was performed with a Magnex Scientific 9.4-T 21-cm-diam horizontal bore magnet with a Magnex gradient coil set capable of achieving 20 G/cm. The diffusion weighted imaging protocol employed a diffusion gradient sampling scheme, which consisted of a keyhole Cartesian acquisition to include q-space values lying on a Cartesian grid (q spacing=0.06 μm^{-1}) within a sphere of radius $q_{\max}=0.3$ μm^{-1}, for a total of 515 sampling points. Assuming a mean sample size of $3\times2\times1$ mm, and employing a $b_{\max}$ value of 7000 s/mm, net voxel size of $150\times150\times150$ μm^3, and a repetition time (TR) of 1200 ms, the image acquisition time was ~22 h per sample.

2.4 *Whole Tissue Imaging with Two-Photon Microscopy*

Tongue tissue specimens were imaged using a multiphoton high-speed imaging system with a robotic sample stage and an automated microtome. The central concepts embodied by the current two-photon microscopic imaging system have been previously described.[19–21] TPM was achieved using a custom-built microscope that incorporated the following elements: a high-speed polygonal scanning mirror achieving a speed approximately 40 times faster than conventional TPM, an automated x-y specimen stage, and an automated tissue-sectioning mechanism. The instrument was developed around a Zeiss microscope (Axioscope, Zeiss Thornwood, NY). A

femtosecond Ti: Sapphire laser, powered by a continuous wave Nd:YLF diode pump laser, (Mira 900, Coherent, Palo Alto, CA) was used to induce two-photon fluorescence providing high-power mode-locked pulses for nonlinear two-photon excitation. The microscope system was optimized for excitation in the range of 700–900 nm. Both the polarization and the excitation power were controlled by a half wave plate (CVI Laser Inc., Putnam, Connecticut) and a Glan-Thomson polarizer. The laser beam is rapidly raster scanned across a sample plane by means of two different scanners. A fast rotating polygonal mirror (Lincoln Laser, Phoenix, AZ) accomplishes high-speed line scanning along the x-axis, and a slower galvanometer-driven scanner with 500 Hz bandwidth (Cambridge Technology, Cambridge, MA) correspondingly deflects the line-scanning beam along the sample's y-axis. The spinning polygonal mirror is composed of 50 aluminum-coated facets arranged contiguously around the perimeter. The facets repetitively deflect the laser beam over a specific angular range and correspondingly scan a line 50 times per revolution.[21] To acquire images at 10 fps, a rotation speed of 3750 rpm was selected corresponding to a line scan speed of 320 μs/line. The pixel residence time was $\sim$0.7 μs. An independent laser diode (1 mW at 632 nm, Thorlabs, Newton, NJ) along with a photodiode detector (Thorlabs) was used to encode the polygonal mirror position and to generate a reference signal. This signal was used by a high-speed data acquisition circuit to synchronize the x-y scanners, the objective translator, and photomultiplier tube (PMT) detection circuitry. The laser beam was coupled with an upright microscope (Axioscope, Zeiss, Thornwood, NY) by means of a modified epiluminescence light path, employing a beam reflected by the dichroic mirror toward the objective and is focused on the specimen. A Zeiss 40× Fluar 1.3 numerical aperture (NA) objective was used in these experiments. Photons were collected using nonspatially resolved detectors (R3896, Hamamatsu, Bridgewater, NJ).

To image areas larger than the field of view of the microscope objective, a robotic stage (H101, Prior Scientific, Rockland MA) was used. Overlaps between the image stacks at adjacent stage locations were maintained at $\sim$30% to facilitate montaging of these images. To acquire 3-D volumes, the objective was mounted on a computer-controlled piezoelectric objective translator (P-722.00, Physik Instrumente, Waldbronn, Germany). Axial translation of the objective in this manner yields a z stack of image planes, with a maximum z-axis travel range of 100 μm. Because the maximum imaging depth of TPM is limited to $\sim$100 μm for an acceptable signal-to-noise ratio, we were able to image the whole organ through a process of successive removal of the tissue layer that had been imaged. The induced fluorescence signal is collected by the same objective and passes through the dichroic mirror. Residual scattered light is removed by an additional barrier filter (SP700, Chroma Technology, Brattleboro, VT). The signals derived from the PMT were converted to a voltage signal using a trans-impedance circuitry and a 16-bit A/D converter (NI 6251, National Instruments Corp., Austin, TX) that operates up to 1.25 million samples per second. The signal is transferred to the computer memory through the PCI bus and images are generated by integrating the signal synchronized with the raster-scanning pattern of the scanners. The net imaging speed is 10 fps for 300×400 pixels using one color channel, and the field of view (FOV) was approximately 140×160 μm^2.

A 3-D autocorrelation algorithm was used to ascertain main fiber directions in microscopic fields of view. This method was based on the obtaining the Fourier transform of the image volume, performing component-by-component multiplication by its own complex conjugate and inverse transforming back into real space.[17] Each FOV was divided into four unique image volumes with dimensions $80\times60\times60$ μm^3. The image volumes were first linearly interpolated in the z direction to give isotropic voxel resolution and windowed with a Kaiser window to reduce edge effects. A spatial frequency filter was applied to remove those features with a spatial period of $\geqslant$120 μm. The main patterns in the microscopy data were revealed by radially integrating from the center of the autocorrelation data, thereby generating an ODF similar to that generated for each voxel using diffusion spectrum MRI. A single value was recorded for the bidirectional radial integration of a set of 181 vectors equally spaced on the surface of a half-sphere; thus, compressing each 9.2-megabyte image volume file into a list 181 numbers.

The goal of the present analysis was to obtain a qualitative comparison of mesoscale (multivoxel) myofiber tract orientation, derived from the principal autocorrelation and diffusion vectors in equivalently sized fields of view. This approach takes advantage of the universal ability of the ODF formulation and myofiber tract generation to represent large arrays of myofibers (across multiple fields of view), thus making the qualitative comparison of the underlying fiber orientation derived from the NMR and optical methods feasible. Because the systematic comparison of individual fields of view would likely be compromised by artifacts associated with the embedding process and subtle nonuniformities in the mechanism by which tissue slicing was performed, such analysis was not attempted in the current study.

3 Results

Through the use of DSI, a diffusion-weighted MR signal is obtained for an indexed array of gradient directions in q space, a probability density function for diffusivity of the imaged space is derived through the Fourier relationship and the resulting pdf is radially integrated to yield the ODF (Fig. 1). Analyses of 3-D microscopy image stacks were accomplished using an autocorrelation algorithm to extract main fiber directions (Fig. 2). The ODF resulting from both methods was then used to compare net fiber orientation at each spatial scale (Fig. 3). In order to infer a higher order (i.e., multivoxel, measure of fiber architecture), we employed tractography, a visualization method that creates graphical associations based on angular similarity of adjacent voxels.[22] Streamline construction through tractography generates multivoxel scale tracts along vectors corresponding to local maxima of the ODF in each voxel.

We display in Fig. 4 the normal myoarchitecture of the excised anterior murine tongue obtained by DSI tractography. These images demonstrate numerous anatomical details previously demonstrated in the case of other mammalian species[23] and as well as several anatomical observations heretofore not described in the case of the mouse. The intrinsic

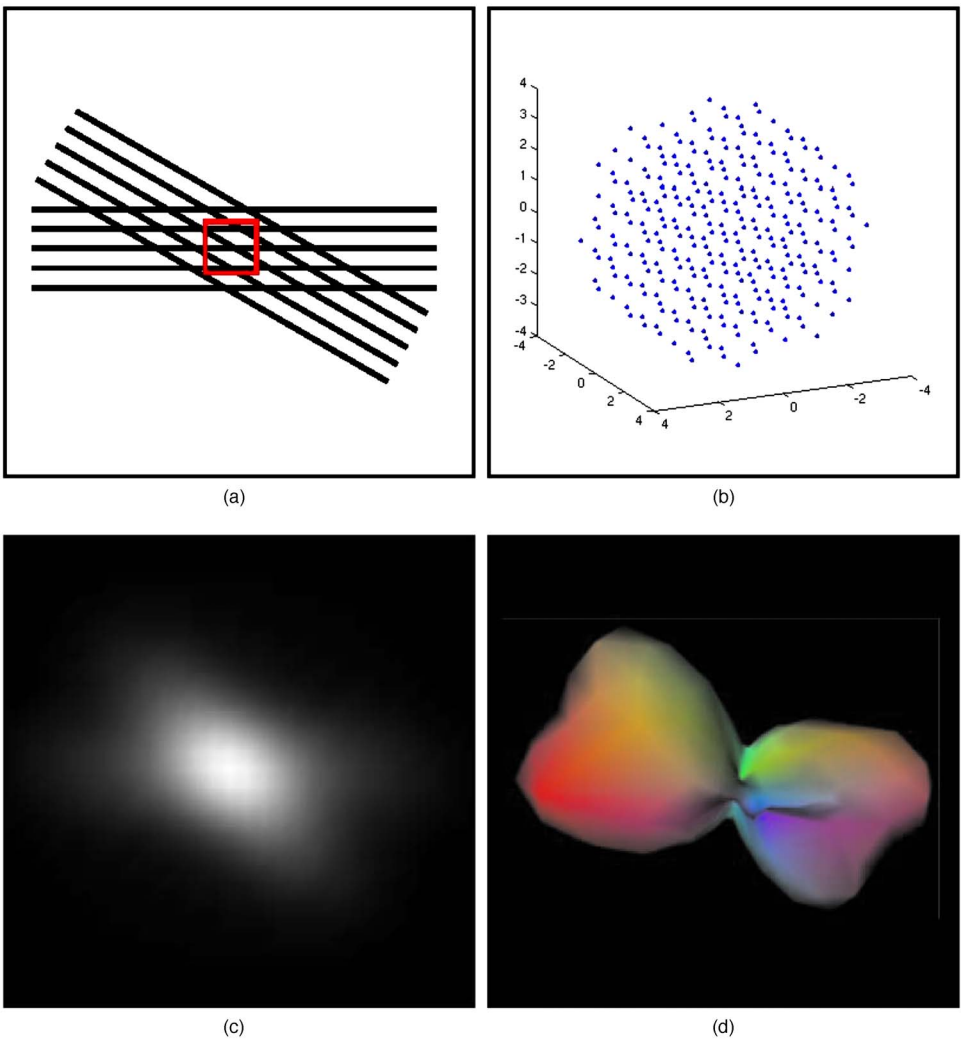

Fig. 1 Derivation of fiber alignment from diffusion spectrum imaging. To extract multiple fiber directions within a voxel (a—red square), diffusion spectrum imaging first acquires a diffusion-weighted signal for an indexed array of gradient directions and magnitudes in *q* space (b). Then, through the Fourier relationship, the pdf is found (c). Lastly, radial integration provides an ODF that mimics the subvoxel fiber alignments (d). (Color online only.)

fibers consist of the superior longitudinalis and inferior longitudinalis, which are positioned along the dorsal and ventral exterior surfaces. The transversus fibers appear to form a concave boxlike structure in the midportion of the tissue, with the verticalis fibers appearing as lateral and obliquely aligned structures. The genioglossus enters from the inferior portion of the tissue and extends along the sagittal plane inserting into the lingual core. Laterally located and longitudinally aligned fibers wrap in the superior direction around the tissue and appear to represent the styloglossus or the mouse equivalent of the chondroglossus.

Figure 5 compares myofiber tractography renderings (sagittal orientation) from DSI (Fig. 5(a)) and from TPM (Fig. 5(b)) for the mouse anterior tongue. The principal patterns in the microscopy data were revealed by radially integrating from the center of the autocorrelation data, thereby creating an ODF similar to that created for each voxel using diffusion spectrum MRI. In this manner, mesoscale tractography was performed both from the exact fiber orientation obtained by microscopy and that obtained by DSI of the whole tissue, thus providing a spatial linkage at the mesoscale. This phenomenon is further illustrated by DSI images displaying myofiber tractography renderings for the specific lingual core region of the lateral transversus at low (Fig. 5(c)) and high (Fig. 5(d)) magnifications, and by TPM images displaying myofiber tractography at similar resolution (Fig. 5(e)) with the corresponding region of lingual myocytes.

4 Discussion

Complex and hierarchical tissue geometries present a unique problem for the determination of structure-function relationships. In order to address this question, a method is needed to translate information of muscle fiber geometry into practical mechanical scales. We present an approach by which such multiscalar structural analyses may be carried out, employing high-field diffusion-based NMR imaging and high-throughput TPM to create comparable volumetric myoarchitectural data

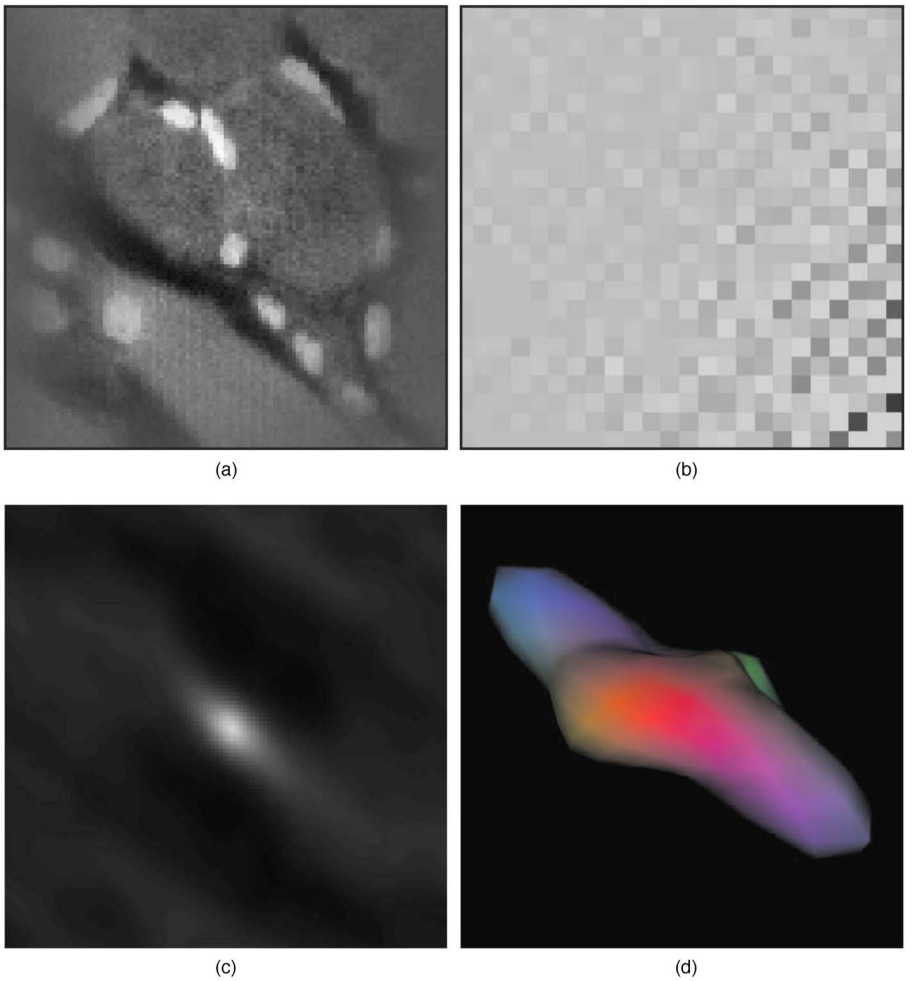

Fig. 2 Derivation of fiber alignment from TPM. To determine fiber directions within a TPM field of view, a 3-D autocorrelation analysis is performed. First, the data are windowed with a Kaiser window (a) to reduce edge effects, then by 3-D Fourier transform, the data are expressed in frequency space (b) and a spatial frequency filter applied to remove patterns with a spatial period greater than or equal to twice the FOV. The 3-D Fourier transform is then multiplied by its own complex conjugate and inverse Fourier transformed to obtain the autocorrelation (c). Lastly, radial integration provides an ODF that describes fiber alignments (d).

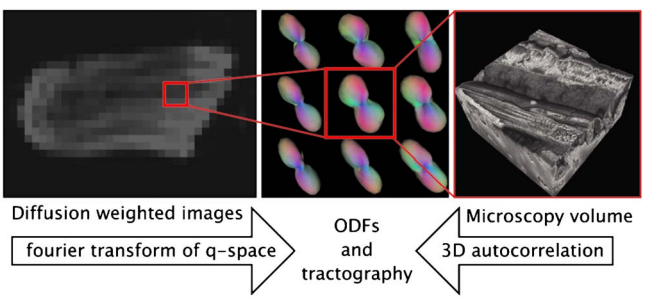

Fig. 3 Mesoscale comparison of fiber orientation obtained from diffusion-weighted NMR and TPM imaging. To quantitatively relate myofiber architecture at the resolution of the cell and the tissue, voxel-specific ODFs and intervoxel tracts were generated. A set of diffusion-weighted images leads to the extraction of subvoxel information about fiber alignment in the form of an ODF field, whereas an ODF field can also be generated directly via the 3-D autocorrelation function of the microscopic image.

in the case of a model tissue, the mouse tongue. We propose that the local ODF derived from these NMR and optical imaging methods represent a mesoscale construct linking the microscopic and macroscopic tissue architectural scales. The analysis of diffusion in a three-dimensionally resolved voxel results in a pdf whose dimensions may be reduced by integrating radially. Similarly, the principal geometric patterns residing in microscopy data may be extracted by radially integrating from the center of a 3-D autocorrelation function. The local maxima of the resulting ODFs in each case may be compiled into a vector field, whose mesoscale orientational patterns may be displayed through streamline tractography. The alignment of the arrayed principal orientation vectors into multivoxel myofiber tracts comprises a method to visually coregister the NMR and optical data sets and, in so doing, perform multiscale comparisons.

By classical anatomical definitions, the lingual musculature is comprised of intrinsic muscles, consisting of a core region of orthogonally related fibers contained within a sheathlike region of longitudinally oriented fibers, which deli-

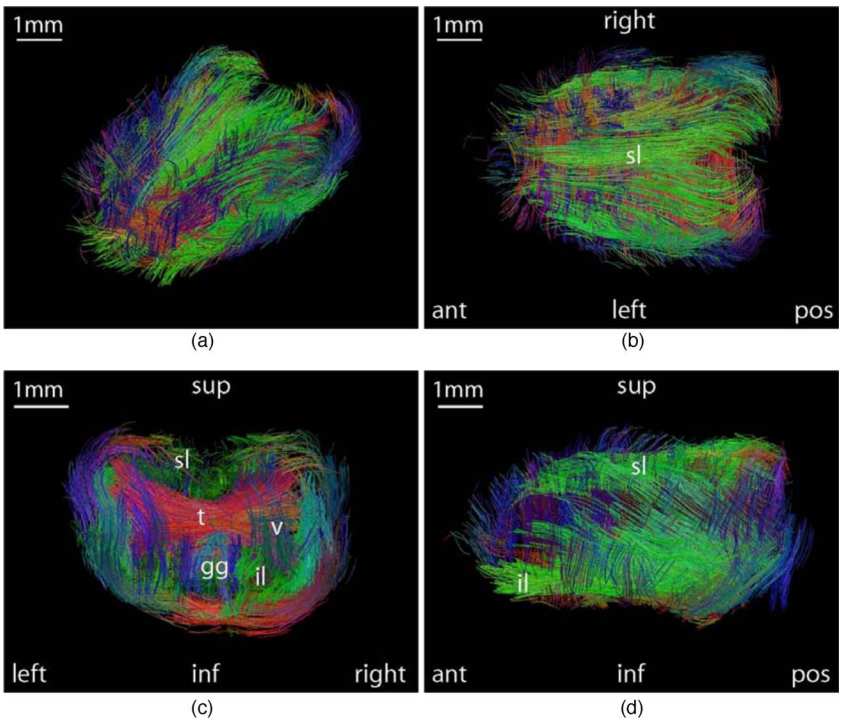

Fig. 4 Myoarchitecture of the mouse tongue demonstrated by DSI tractography. Demonstrated is a full DSI with tractography data set obtained at 9.4 T (voxel size 150 μm) of the anterior 357BL mouse tongue from the (a) oblique, (b) coronal (superior), (c) axial (posterior), and (d) sagittal perspectives. The green superior longitudinalis (sl) and inferior longitudinalis (il) run along the dorsal and ventral exterior surfaces. The transversus (t) and verticalis (v) are not perfectly horizontal and vertical but rather form an interesting concave boxlike structure, becoming parallel with each other at the corners. Extrinsic fibers identified include the genioglossus (gg) and palatoglossus (pg). A scale bar is provided for each image. (Color online only.)

cately merge with extrinsic fibers that modify shape and position from the superior (palatoglossus), posterior (styloglossus), and inferior (hyoglossus and genioglossus) directions. However, structural analysis of lingual myoarchitecture suggest that partitioning of the tongue into nominally discrete muscles may be inaccurate and that the lingual musculature may better be conceived as a continuous array of elements. Employing the proposed method, the structural components of each element may be considered as a hierarchical organization of individual myofibers and fiber arrays, allowing the tissue to be defined simultaneously at the microscopic (individual myofiber), mesoscopic (multifiber arrays), and macroscopic (whole tissue) scales.

Diffusion-weighted NMR methods define muscular anatomy as an array of elements representing directional differences of molecular diffusion.[24] Because maximal diffusion occurs parallel to the long axis of most fiber-type cells, diffusion measurements can be used to define 3-D fiber orientation. Our initial studies exploited diffusion tensor fields[12] to study myoanatomy in terms of the principal direction of the contained fibers, an approach validated on the basis of the 3-D autocorrelation for individual fields of view obtained by TPM.[17] By this analysis, we defined the structural heterogeneity of the lingual core as a series of discrete regions of in-plane parallel fibers, with a measurable degree of angular separation recapitulating the macroscopic angular separation displayed by MRI. To address inaccuracies in assessing fiber direction in the case of intravoxel crossing, we developed DSI, which determines the alignment of geometrically heterogeneous fiber populations by deriving the complete 3-D spin-displacement function per voxel, and yields an ensemble pdf for the complete set of possible molecular displacements.[6,7] In order to relate the tissue's highly complex myoarchitecture with the myriad possible deformations occurring during physiological motion, we employed streamline tractography to align similar vector directions and thus generate mesoscale myofiber tracts,[8] whose length and orientation are believed to constitute structural templates for local contractility. In the current study, we have extended this methodology to a considerably higher resolution (voxel size of $\sim 100\ \mu m^3$) at 9.4 T. In so doing, we have confirmed previous concepts involving the merged architecture of the intrinsic and extrinsic fiber populations of the mammalian tongue and have determined a novel fiber configuration for the transversus and verticalis fibers of the intrinsic core of the tongue specific to the mouse model. Moreover, owing to the fact that the achievable voxel size is equivalent to the FOV obtained by TPM, high-field DSI provides a direct basis for microscopic correlation.

TPM is a 3-D imaging technique based on the nonlinear excitation of fluorophores.[19,20] For purposes of 3-D imaging: (*i*) TPM provides optimal depth discrimination based on the quadratic dependence of two-photon fluorescence intensity upon the excitation photon flux, which decreases rapidly away from the focal plane. (*ii*) The longer wavelengths employed in TPM have significantly lower scattering and absorption and

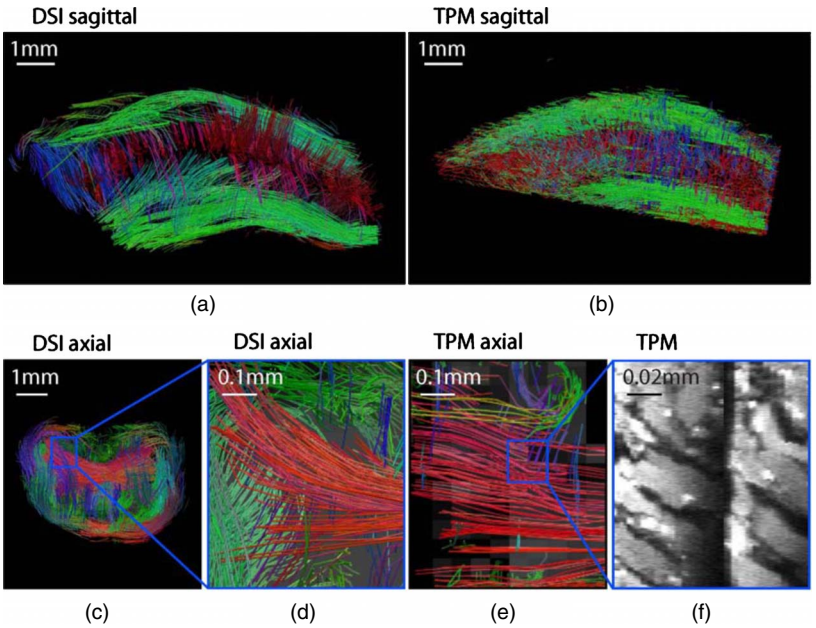

Fig. 5 Comparison of mesoscale tractography rendering derived from DSI and TPM. Upper row: Tractography of mouse tongue myoarchitecture (sagittal orientation) obtained by DSI (a) and TPM (b). The most lateral slices of the DSI tractography have been removed to match the TPM. DSI tractography image (c) of an axial slice and a close-up (d), emphasizing the transverse-oriented fibers. Similar resolution TPM tractography image is displayed (e) accompanied by a TPM image in (f) of a region of myocytes corresponding to the indicated myofiber tracts shown in (e, blue square). These results confirm the capacity of these imaging methods to derive equivalent intermediate scale myofiber tracts from the local diffusion maxima displayed by DSI and directly from 3-D microscopy data. A scale bar is provided for each image. (Color online only.)

thus enhance tissue penetration. (*iii*) TPM causes minimal photodamage to biological specimens because photoactivation is restricted to the subfemtoliter focal volume. In the current configuration, we additionally incorporated a video rate two-photon system based on the raster scanning of a single diffraction limited focal spot using a high-speed polygonal mirror[24] and an automated tissue sectioning mechanism to allow the complete 3-D sampling of the whole tissue in a practical time frame. To address myoarchitecture in microscopic data sets, we adopted the 3-D autocorrelation formalism to derive fiber orientation per sampled volume. By radially integrating from the center of the autocorrelation data, we generate an ODF similar in scale to that generated with DSI.

Because the output of both the optical and NMR imaging methods combines at the scale of the ODF, we were able to compare the architectural features of the tongues imaged by each method. In the ideal circumstance, where cells possess perfectly reflexive boundaries and diffusion time is allowed to be infinite, the 3-D autocorrelation function should precisely predict the NMR pdf for a given diffusional compartment. Although our data infers the similarity of these functions, this cannot be absolutely known because the physical barriers that shape the diffusion function are not completely understood[25] and infinite diffusion times are impractical. Acknowledging this limitation, derivation of the ODF obtained through either optical or NMR methods provides a method for reliably comparing fiber orientation at intermediate spatial scales. The derivation of mesoscale structures from microscopic data may in turn provide a structural blueprint for local contractility and, thus, an anatomical point of reference for the simulation of mechanical performance in complex tissues.

5 Conclusion

In conclusion, we have derived 3-D fiber orientation in the mouse tongue through two physically distinct methods that merge spatially as an ODF resulting alternatively from the display of local diffusion maxima (DSI) or the mean microscopic fiber orientation (TPM). Comparison of these methods was performed based on the distribution of mesoscale myofiber tracts generated from the vector fields associated with each data set and demonstrated qualitatively the superimposition of the distributed mesoscale myofiber tracts. The identification of the cells comprising mesoscale myoarchitecture of a given tissue thus provides a method for relating information on the microscopic scales with the morphology and mechanics of whole tissues. Spectroscopic information obtained with microscopic imaging may further elucidate the molecular origin of certain muscular pathologies. For example, the SHG signal from semicrystalline myosin structures may infer the etiology of muscular dystrophy,[26,27] ascertain the basis of tissue contractility,[28] or reveal sarcomere disruption.[29] By linking such cellular and molecular scale information with tissue scale myoarchitecture and mechanics, it may thus be feasible to consider multiscale models[30] of normal and pathological organ function.

References

1. R. J. Gilbert, V. J. Napadow, and V. J. Wedeen, "Anatomical basis for lingual hydrostatic function," *J. Exp. Biol.* **210**(23), 4069–4082 (2007).
2. K. C. Nishikawa, W. M. Kier, and K. K. Smith, "Morphology and mechanics of tongue movement in the African pig-nosed Hemisus Marmoratum: A muscular hydrostatic model," *J. Exp. Biol.* **202**, 771–

780 (1999).
3. D. D. Streeter, H. M. Spotnitz, D. P. Patel, J. Ross, and E. H. Sonnenblick, "Fiber orientation in the canine left ventricle during diastole and systole," *Circ. Res.* **24**, 339–347 (1969).
4. R. T. Megens, S. Reitsma, P. H. Schiffers, R. H. Hilgers, J. G. De Mey, D. W. Slaaf, M. G. Oude Egbrink, and M. A. van Zandvoort, "Two-photon microscopy of vital murine elastic and muscular arteries. Combined structural and functional imaging with subcellular resolution," *J. Vasc. Res.* **44**(2), 87–98 (2007).
5. R. J. Gilbert, T. A. Gaige, T. Benner, R. Wang, G. Dai, J. N. Glickman, and V. J. Wedeen, "Resolving the three dimensional myoarchitecture of the bovine esophageal wall with diffusion spectrum imaging and tractography," *Cell Tissue Res.* **332**(3), 461–468 (2008).
6. R. J. Gilbert, L. H. Magnusson, V. J. Napadow, T. Benner, R. Wang, and V. J. Wedeen, "Mapping complex myoarchitecture in the bovine tongue with diffusion spectrum magnetic resonance imaging," *Biophys. J.* **91**(3), 1014–1022 (2006).
7. V. J. Wedeen, T. Reese, D. Tuch, M. Wiegell, J. Dou, R. Weisskoff, and D. Chessle, "Mapping fiber orientation spectra in cerebral white matter with Fourier-transform diffusion MRI," presented at 8th Annual Meet. of Int. Soc. of Magnetic Resonance Med. Denver, 2000.
8. R. J. Gilbert, V. J. Wedeen, L. H. Magnusson, T. Benner, R. Wang, G. Dai, V. J. Napadow, and K. K. Roche, "Three-dimensional myoarchitecture of the bovine tongue demonstrated by diffusion spectrum magnetic resonance imaging with tractography," *Anat. Rec. A Discov. Mol. Cell Evol. Biol.* **288**(11), 1173–1182 (2006).
9. T. Ragan, J. D. Sylvan, K. H. Kim, H. Huang, K. Bahlmann, and R. T. Lee, "High-resolution whole organ imaging using two-photon tissue cytometry," *J. Biomed. Opt.* **12**(1), 014015 (2007).
10. D. G. Cory and A. N. Garroway, "Measurement of translational displacement probabilities by NMR: An indicator of compartmentation," *Magn. Reson. Med.* **14**(3), 435–444 (1990).
11. P. G. Campagnola and L. M. Loew, "Second harmonic imaging microscopy for visualizing biomolecular arrays in cells, tissues, and organisms," *Nat. Biotechnol.* **21**(11), 1356–1360 (2003).
12. V. J. Wedeen, T. G. Reese, V. J. Napadow, and R. J. Gilbert, "Demonstration of primary and secondary fiber architecture of the bovine tongue by diffusion tensor magnetic resonance imaging," *Biophys. J.* **80**, 1024–1028 (2001).
13. T. A. Gaige, T. Benner, R. Wang, V. J. Wedeen, and R. J. Gilbert, "Three dimensional myoarchitecture of the human tongue determined in vivo by high resolution diffusion tensor imaging with tractography," *J. Magn. Reson Imaging* **26**(3), 654–661 (2007).
14. V. J. Napadow, Q. Chen, V. J. Wedeen, and R. J. Gilbert, "Intramural mechanics of the human tongue in association with physiological deformations," *J. Biomech.* **32**, 1–12 (1999).
15. V. J. Napadow, Q. Chen, V. J. Wedeen, and R. J. Gilbert, "Biomechanical basis for lingual tissue deformation during swallowing," *Am. J. Physiol.* **40**, G695–G701 (1999).
16. V. J. Napadow, R. D. Kamm, and R. J. Gilbert, "Biomechanical model of sagittal bending for the human tongue," *J. Biomech. Eng.* **124**, 547–556 (2002).
17. V. J. Napadow, Q. Chen, V. Mai, P. T. C. So, and R. J. Gilbert, "Quantitative analysis of 3D resolved fiber architecture in heterogeneous skeletal muscle using NMR and optical imaging methods," *Biophys. J.* **80**, 2968–2975 (2001).
18. E. Stejskal and J. Tanner, "Use of spin echoes in a pulsed magnetic field gradient to study anisotropic restricted diffusion and flow," *J. Chem. Phys.* **43**, 3597–3603 (1965).
19. P. T. C. So, C. Y. Dong, B. Masters, and K. M. Berland, "Two-photon excitation fluorescence microscopy," *Annu. Rev. Biomed. Eng.* **2**, 399–429 (2000).
20. F. Helmchen and W. Denk, "Deep tissue two-photon microscopy," *Nat. Methods* **2**(12), 932–940 (2005).
21. K. H. Kim, C. Buehler, and P. T. C. So, "High-speed, two-photon scanning microscope," *Appl. Opt.* **38**(28), 6004–6009 (1999).
22. P. J. Basser, S. Pajevic, C. Pierpaoli, J. Duda, and A. Aldroubi, "*In vivo* fiber tractography using DT-MRI data," *Magn. Reson. Med.* **44**(4), 625–632 (2000).
23. G. Toure and C. Vacher, "Anatomic study of tongue architecture based on fetal histological sections," *Surg. Radiol. Anat.* **28**, 547–552 (2006).
24. P. J. Basser, J. Mattiello, and D. LeBihan, "MR diffusion tensor spectroscopy and imaging," *Biophys. J.* **66**, 259–267 (1994).
25. H. Zhang, Y. Xie, and T. Ji, "Water diffusion-exchange effect on the paramagnetic relaxation enhancement in off-resonance rotating frame," *J. Magn. Reson.* **186**(2), 259–272 (2007).
26. S. V. Plotnikov, A. C. Millard, P. J. Campagnola, and W. A. Mohler, "Characterization of the myosin-based source for second-harmonic generation from muscle sarcomeres," *Biophys. J.* **90**(2), 693–703 (2006).
27. M. Both, M. Vogel, O. Friedrich, F. von Wegner, T. Künsting, R. H. Fink, and D. Uttenweiler, "Second harmonic imaging of intrinsic signals in muscle fibers in situ," *J. Biomed. Opt.* **9**(5), 882–892 (2004).
28. T. Boulesteix, E. Beaurepaire, M. P. Sauviat, and M. C. Schanne-Klein, "Second-harmonic microscopy of unstained living cardiac myocytes: measurements of sarcomere length with 20-nm accuracy," *Opt. Lett.* **29**(17), 2031–2033 (2004).
29. C. Greenhalgh, N. Prent, C. Green, R. Cisek, A. Major, B. Stewart, and V. Barzda, "Influence of semicrystalline order on the second-harmonic generation efficiency in the anisotropic bands of myocytes," *Appl. Opt.* **46**(10), 1852–1859 (2007).
30. P. Hunter and P. Nielsen, "A strategy for integrative computational physiology," *Physiology (Bethesda)* **20**, 316–325 (2005).